Fractional topological phases in generalized Hofstadter bands with arbitrary Chern numbers

Ying-Hai Wu, J. K. Jain, and Kai Sun

Fractional Topological Phases in Generalized Hofstadter Bands
with Arbitrary Chern Numbers

Ying-Hai Wu[1], J. K. Jain,[1] and Kai Sun[2]

[1] *Department of Physics, The Pennsylvania State University, University Park, PA 16802, USA*
[2] *Department of Physics, University of Michigan, Ann Arbor, MI 48109, USA*
(Dated: October 30, 2014)

We construct generalized Hofstadter models that possess "color-entangled" flat bands and study interacting many-body states in such bands. For a system with periodic boundary conditions and appropriate interactions, there exist gapped states at certain filling factors for which the ground state degeneracy depends on the number of unit cells along one particular direction. This puzzling observation can be understood intuitively by mapping our model to a single-layer or a multi-layer system for a given lattice configuration. We discuss the relation between these results and the previously proposed "topological nematic states", in which lattice dislocations have non-Abelian braiding statistics. Our study also provides a systematic way of stabilizing various fractional topological states in $C > 1$ flat bands and provides some hints on how to realize such states in experiments.

Introduction — The topological structure of two-dimensional space plays an fundamental role in understanding the quantum Hall effect [1, 2]. It was proved by Thouless *et. al.* [3] that, for a system of non-interacting electrons, the Hall conductance is proportional to the Chern number C defined as the integral of Berry curvature over the Brillouin zone (BZ) [4]. This clarifies the topological origin of the integer quantum Hall effect because the Landau levels generated in an uniform magnetic field all have $C = 1$. Haldane demonstrated subsequently that an uniform external magnetic field is not necessary by showing that a two-band model on honeycomb lattice with suitable parameters can have $C = \pm1$ bands [5]; such systems are now termed "Chern insulators" [6–8]. When interactions between particles in a partially filled Landau level are taken into account, fractional quantum Hall (FQH) states can appear at certain filling factors. For a sufficiently flat band with a nonzero Chern number, fractional topological states may also be realized for suitable interactions [9–29]. Many states in $C = 1$ flat bands are shown to be adiabatically connected to those in Landau levels [24–26], which provides a simple way of characterizing their properties.

In constrast to a Landau level which has $C = 1$, a topological flat band can have an arbitrary Chern number. This motivates one to ask what is the nature of the fractional topological phases in $C > 1$ flat bands [30–34] and whether it is possible to realize some states that may not have analogs in conventional Landau levels. Ref. [35] demonstrates that the incompressible ground states in a $C > 1$ flat band at filling factor $\nu = 1/(C + 1)$ [$\nu = 1/(2C + 1)$] for bosons (fermions) can be interpreted as Halperin states [36] with special flux insertions (*i.e.* boundary conditions) in *some* cases, but the nature of other states remains unclear. Ref. [37] proposed that some bilayer FQH states would have special properties if they are realized in $C = 2$ systems and dubbed them as "topological nematic states", but numerical evidence for such states has not been found. In this Letter, we construct generalized Hofstadter models and demonstrate that there are interacting systems whose ground state degeneracy (GSD) depends on the number of unit cells along one direction. It is found that our models can be mapped either to a single-layer or to a multi-layer quantum Hall system depending on the lattice configuration, which provides a simple physical picture that helps us to understand the puzzling properties of $C > 1$ flat bands. The change of GSD is one signature of the topological nematic states [37], but there are other subtle issues, *e.g.* qualitative differences between bosons and fermions and the nature of the symmetry reduction, which we explain using our models.

Color-Entangled Hofstadter Models — We construct flat bands with arbitrary Chern numbers by generalizing the Hofstadter model [38–42] using the generic scheme of Ref. [32]. As shown in Fig 1 (a), the Hofstadter model describes particles in both a uniform magnetic field and a periodic potential. The tight-binding Hamiltonian for the model on a square lattice is $H = \sum_{ij} t_{ij} e^{i\theta_{ij}} \widehat{a}_i^\dagger \widehat{a}_j + \text{H.c.}$, where θ_{ij} is the phase associated with the hopping from site j to i [38], $\widehat{a}_i^\dagger$ is the creation operator on site i and H.c. means Hermitian conjugate. If the magnetic flux per plaquette is $2\pi/n_\phi$ with n_ϕ being an integer, translational symmetry is preserved on the scale of magnetic unit cell which contains n_ϕ plaquettes. The momentum space Hamiltonian is $H(\mathbf{k}) = \Psi^\dagger(\mathbf{k})\mathcal{H}\Psi(\mathbf{k})$, where $\Psi^\dagger(\mathbf{k}) = [\widehat{a}_0^\dagger(\mathbf{k}), \widehat{a}_1^\dagger(\mathbf{k}), \cdots, \widehat{a}_{n_\phi-1}^\dagger(\mathbf{k})]$ and the subscript of $\widehat{a}^\dagger$ marks different sites within a magnetic unit cell. $\mathcal{H}(\mathbf{k})$ is a $n_\phi \times n_\phi$ matrix whose non-zero matrix elements are $\mathcal{H}_{mm}(\mathbf{k}) = 2\cos(k_y + 2m\pi/n_\phi)$ and $\mathcal{H}_{mn}(\mathbf{k}) = \mathcal{H}_{nm}^*(\mathbf{k}) = \exp(ik_x/n_\phi)$ for $n = (m + 1) \bmod n_\phi$. The $n_\phi \to \infty$ limit recovers the continuous limit in which Landau levels arise. One important advantage of starting from the Hofstadter model is that the Berry curvature of the lowest band can be made uniform over the entire BZ. This is desirable because a nonuniformity in the Berry curvature usually tends to weaken or even destroy
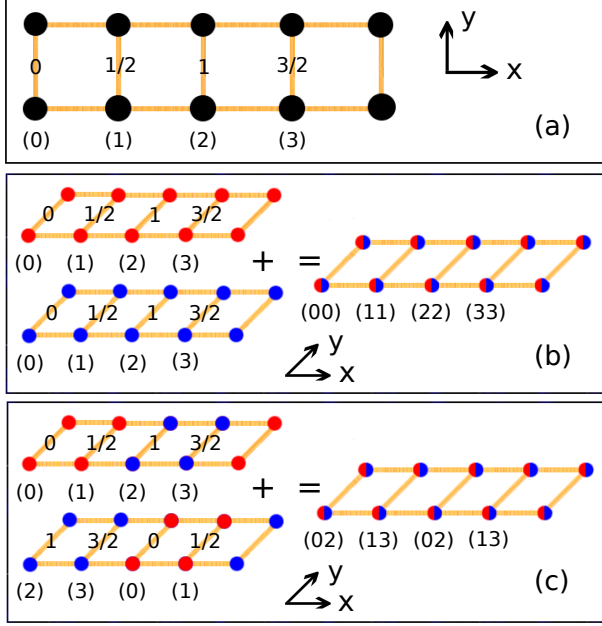
FIG. 1. (color online) In panel (a), we give an example of Hofstadter lattice with $n_\phi = 4$ that are used in panels (b) and (c). The indices of orbitals in a magnetic unit cell are shown in parentheses and the numbers on the bonds indicate the phases of the complex hopping amplitudes along the y direction in units of π. In panel (b), a bilayer Hofstadter model is obtained by stacking the two layers together. In panel (c), the two Hofstadter layers are shifted relative to each other and then stacked together. The method used in panel (c) gives a color-entangled Hofstadter model in which the size of the magnetic unit cell is reduced by a factor of two and the lowest band has $C = 2$. There are two orbitals on each lattice site (colored in red and blue) for both models and their indices are given in parentheses.

incompressible states [24].

We next stack two identical Hofstadter lattices together in two different ways. In Fig. 1 (b), the same orbitals in different layers are aligned together, which results in a conventional bilayer quantum Hall system. In Fig. 1 (c), the m-th orbital in one layer is aligned with the $(m+n_\phi/2)$-th orbital in the other layer. The latter stacking pattern reduces the size of the magnetic unit cell by half [32], so the model shown in Fig 1 (c) possess a single lowest band with $C = 2$ instead of having two degenerate $C = 1$ bands. It should be emphasized that these two systems are equivalent insofar as the behavior of the *bulk* is concerned, since they correspond to two different gauge choices. However, as shown below, they behave differently when periodic boundary conditions (PBCs) are imposed because PBCs are not invariant under a change of gauge. In general, one can get a band with an arbitrary Chern number C by stacking C layers of Hofstadter lattices and aligning the orbitals labeled by m, $m + n_\phi/C, \cdots$, and $m + (C-1)n_\phi/C$ in different layers (where $m \in [0, 1, \cdots, n_\phi/C - 1]$). The momentum space

Hamiltonian is very similar to the single-layer Hofstadter model, except that the off-diagonal term $\mathcal{H}_{mn}(\mathbf{k})$ is replaced by $\exp(ik_x C/n_\phi)$. A detailed comparison reveals the similarity of the "color-entangled Bloch basis" [35] and our models [43], which suggests that our models, as well as those constructed in Ref. [32], can be referred to as "color-entangled" topological flat band models.

Interacting Many Body Systems — The differences between a bilayer Hofstadter model and a $C = 2$ color-entangled Hofstadter model become transparent when one studies interacting many body systems. We consider N particles on a periodic lattice with N_x and N_y magnetic unit cells along the x and y directions. The total number of plaquettes (to be distinguished with the numbers of magnetic unit cells) along the x and y directions are denoted as L_x and L_y, respectively. The magnetic unit cell is always chosen to contain only one plaquette in the y direction so we have $L_y = N_y$. It was proposed in Ref. [37] that the following bilayer quantum Hall wave functions

$$\Psi_B(\{z^1\}, \{z^2\}) = \Phi_{\frac{p}{p+1}}(\{z^1\})\Phi_{\frac{p}{p+1}}(\{z^2\}) \qquad (1)$$

$$\Psi_F(\{z^1\}, \{z^2\}) = \prod_{i<j}(z_i^1 - z_j^1)^3 \prod_{i<j}(z_i^2 - z_j^2)^3$$
$$\times \prod_{i,j}(z_i^1 - z_j^2) \qquad (2)$$

are topological nematic states in $C = 2$ bands, where $z = x + iy$ is the complex coordinate and its superscript indicates the layer it resides in. Eq. (1) describes bosonic systems with two decoupled layers and Eq. (2) is the Halperin 331 state [36] for fermions. The value of p is chosen to be 1 or 2 and the associated wave functions are the Laughlin 1/2 state $\Phi_{1/2}(\{z^\alpha\})$ and the Jain 2/3 state $\Phi_{2/3}(\{z^\alpha\})$ (they are the bosonic analogs of the Laughlin 1/3 state [44] and the Jain 2/5 state [45] for fermions). When the states represented by Eq. (1) and Eq. (2) are realized on a torus with PBCs, the GSDs are $(p+1)^2$ and 8 respectively [46, 47].

The wave functions Eq. (1) and Eq. (2) can be realized in a bilayer Landau level system in continuum when intra-layer interaction is stronger than inter-layer interaction. This motivates us to study the Hamiltonians $H_B = \sum_i \sum_\sigma U_{\sigma\sigma}^B : \hat{n}_i(\sigma)\hat{n}_i(\sigma) : + \sum_i \sum_{\sigma \neq \tau} V_{\sigma\tau}^B : \hat{n}_i(\sigma)\hat{n}_i(\tau) :$ and $H_F = \sum_{\langle ij \rangle} \sum_\sigma U_{\sigma\sigma}^F : \hat{n}_i(\sigma)\hat{n}_j(\sigma) : + \sum_i \sum_{\sigma \neq \tau} V_{\sigma\tau}^F : \hat{n}_i(\sigma)\hat{n}_i(\tau) :$, where $: \cdots :$ enforces normal ordering, $\hat{n}_i(\sigma)$ is the number operator for particle of color σ on site i, and $\langle ij \rangle$ denotes nearest neighbors. The parameters are chosen as $U_{\sigma\sigma}^B = 1$, $V_{\sigma\tau}^B = 0.03$, $U_{\sigma\sigma}^F = 1$ and $V_{\sigma\tau}^F = 0.5$. In other words, we use intra-color onsite interactions for bosonic systems (with a small perturbation given by the $V_{\sigma\tau}^B$ terms [48]) and both intra-color NN and inter-color onsite interactions for fermionic systems. The eigenstates of these Hamiltonians are labeled by their momenta K_x and K_y along the two directions.
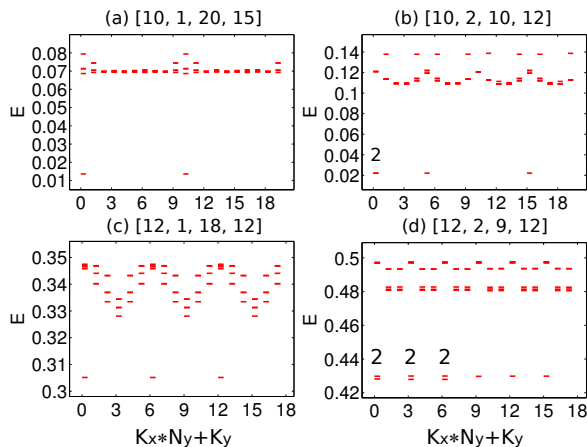
FIG. 2. Energy spectra of bosons on the $C = 2$ model at filling factors $1/2$ [(a) and (b)] and $2/3$ [(c) and (d)]. The system parameters are given in square brackets as $[N, N_x, N_y, L_x]$. The numbers above some energy levels indicate degeneracies that may not be resolved by inspection.
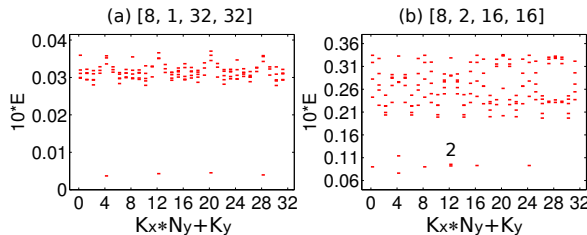

FIG. 3. Energy spectra of fermions on the $C = 2$ model at filling factor $1/4$. The system parameters are given in square brackets as $[N, N_x, N_y, L_x]$. The numbers above some energy levels indicate degeneracies that may not be resolved by inspection.

The many-body Hamiltonians are projected into the partially occupied lowest band(s) [10] and the filling factor is defined as $\nu = N/(\mathcal{M} N_x N_y)$, where $\mathcal{M}$ is the number of bands that are kept in the projection (i.e., $\mathcal{M} = 2$ for the bilayer Hofstadter model and $\mathcal{M} = 1$ for the $C = 2$ color-entangled Hofstadter model). This means that Eq. (1) and Eq. (2) have filling factors $p/(p+1)$ and $1/4$ respectively.

The number of plaquettes in the x direction for given N_x and N_y values is chosen to ensure that this system is close to isotropic (i.e. has aspect ratio close to 1). As the size of the unit cell increases, the wave function of a particle spreads over a larger area and the interaction between two particles becomes weaker. To compare systems with different n_ϕ, we normalize the energy scale using the total energy of two particles in a system with $N_x = 1$ and $N_y = 1$ ($N_x = 1$ and $N_y = 2$) for bosons (fermions).

The GSDs of Eq. (1) and Eq. (2) given above were derived using the continuum wave functions, but we have found that they are still valid for bosonic systems with

Hamiltonian H_B and fermionic systems with Hamiltonain H_F in the bilayer Hofstadter model. The results in the $C = 2$ color-entangled Hofstadter model are very different as presented in Fig. 2 and Fig. 3. The special feature of the $C = 2$ systems is that the GSD depends on N_x and it only agrees with the result in the bilayer Hofstadter model when N_x is even. For bosonic systems, the GSD at $1/2$ is 2 if N_x is odd and 4 if N_x is even; the GSD at $2/3$ is 3 if N_x is odd and 9 if N_x is even. The gaps of the bosonic states survive in the presence of small inter-color onsite interaction $V_{\sigma\tau}^B$ but disappear if $V_{\sigma\tau}^B$ becomes comparable to $U_{\sigma\tau}^B$. The phase boundary can not be determined precisely because a reliable finite-size scaling is difficult here. For fermionic systems, the GSD is 4 for $N_x = 1$ and 8 for $N_x = 2$. The quasi-degenerate ground states have a more prounced splitting than the bosonic cases. The gaps become less clear for larger N_x and there is no well-defined set of quasi-degenerate ground states when $N = 8$, $N_x = 4$, $N_y = 8$, and $L_x = 16$.

Boundary Conditions, Topology, and Symmetry — The key to understanding the physics of a $C = 2$ band is that it may have two fundamentally distinct topologies determined by the parity of N_x. As illustrated in Fig. 4, this originates from the twisted hoppings along the x direction at the boundary between two magnetic unit cells (i.e. the color index of a particle is flipped). For odd N_x [Fig. 4 (a)], it can be unfolded to produce a single Hofstadter layer with $C = 1$ by tracking the black lines which represent hopping terms along the x direction. For even N_x [Fig. 4 (b)], it contains two decoupled Hofstadter layers each having $C = 1$. This mapping is sufficient to explain why the GSD change in the bosonic systems: a single-layer $p/(p+1)$ state with GSD $p+1$ is realized for odd N_x, while two decoupled $p/(p+1)$ states with GSD $(p+1)^2$ appear when N_x is even. The fermionic case is more complicated, but it was argued that the GSD of the Halperin 331 state in a $C = 2$ band is 8 when N_x is even and 4 if N_x is odd [37].

The fact that the unfolding of the model depends only on the parity of N_x but not of N_y signifies a reduction of rotational symmetry. However, in our systems the C_4 symmetry is not broken spontaneously, as in previously studied nematic states [49, 50], but results from the model Hamiltonian itself through boundary conditions. To gain insight into this issue, we note that the simple square lattice Hofstadter model has four-fold rotational symmetry C_4 (up to gauge transformations) even though a magnetic unit cell usually has only two-fold rotational symmetry C_2. This conclusion is valid when the system contains an integral number of magnetic unit cells, which is also satisfied automatically for a Hofstadter mutli-layer. In contrast, since the unit cell of the color-entangled $C = 2$ Hofstadter model is half as large as the original magnetic unit cell, the C_4 symmetry of the parent Hofstadter model is inherited only when N_x is even, but is reduced to C_2 symmetry for odd N_x.
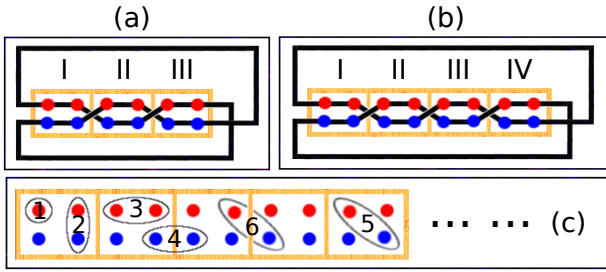
FIG. 4. (color online) This figure shows a slice of the $C = 2$ model constructed in Fig. 1 but the two orbitals are plotted separately for clarity. In panels (a) and (b), the unit cells are labeled by Roman numbers and the black lines represent the hopping terms along the x direction. When N_x is odd in (a) [even in (b)], this model maps into a single-layer (bilayer) system. The hopping terms along the y direction do not change this mapping. Panel (c) shows certain interaction terms: 1. intra-color onsite term; 2. inter-color onsite term; 3. intra-color NN term within one unit cell; 4. intra-color NN term across the boundary of a unit cell; 5. inter-color NN term within one unit cell; 6. inter-color NN term across the boundary of a unit cell.

Although the GSDs of bosonic systems confirm the theoretical predictions, the fermionic 331 state seems less stable. This puzzle is resolved when we analyze the 2-body interaction terms shown in Fig. 4 (c), which also have different effects depending on the parity of N_x. For both even and odd N_x, the term (1) in Fig. 4 (c) is still an onsite term and both (3) and (6) turn out to be intra-layer nearest neighbor (NN) terms. If N_x is even, (2), (4) and (5) become, respectively, an inter-layer onsite term, an inter-layer NN term, and an inter-layer NN term. On the other hand, when N_x is odd, (2), (4) and (5) all result in interactions, in the single unfolded layer, that extend over a range comparable to the system size. In a fermionic system with even N_x, the intra-color NN terms across boundaries between unit cells turn into inter-layer NN terms when the model is mapped to a bilayer system, which is expected to weaken or destroy the 331 state. If one carefully design the Hamiltonian to make sure that it contains no inter-layer NN terms after mapping into a bilayer system, then one can get a 331 state with a clear gap [51]. The nature of the gapped ground states observed in previous works [31–34] can be better understood in light of these observations [43]. After resolving a subtle issue in the square lattice $C = 2$ model [32], we demonstrate that change of GSD can also be seen in this model [43].

How relevant is the above analysis using PBCs for real physical systems with open boundaries? The topology of a lattice is determined by N_x because the hoppings along the x direction at each boundary between two magnetic unit cells flip the color indices of particles. It was proposed that edge dislocations have a similar effect [37] and they have *projective* non-Abelian braiding statistics [52]:

there are multiple degenerate states given a fixed configuration of dislocations; an exchange of two dislocations results in a unitary evolution in this degenerate space; two such exchanges may not commute with each other; the overall phases of the braiding operations are undetermined. These exotic properties may be demonstrated in tunneling and interferometric measurements [53]. The physics of defects in various topological phases have also been studied [54–57].

We finally briefly mention possible experimental realizations of the fractional topological phases studied above. A variety of proposals for creating synthetic gauge fields for cold atoms have been studied [58, 59] and the complex hoppings in the standard Hofstadter model have been successfully implemented [60, 61]. The feasibility of simulating topological phases using photons has also been investigated [62–69]. The standard Hofstadter model and its time-reversal symmetric variant have been demonstrated for non-interacting photons [70–73]. In view of these achievements and following similar lines of thought, we discuss how color-entangled Hofstadter models with $C > 1$ bands may be realized [43].

In conclusion, we have constructed color-entangled Hofstadter models with arbitrary Chern numbers and demonstrated the existence of fractional topological phases in such systems by extensive exact diagonalization studies. The models we use help to clarify many aspects of topological flat bands with $C > 1$ in a physically intuitive manner.

[1] K. v. Klitzing, G. Dorda, and M. Pepper, Phys. Rev. Lett. **45**, 494 (1980).

[2] D. C. Tsui, H. L. Stormer, and A. C. Gossard, Phys. Rev. Lett. **48** 1559 (1982).

[3] D. J. Thouless, M. Kohmoto, M. P. Nightingale, and M. den Nijs, Phys. Rev. Lett. **49**, 405 (1982).

[4] B. Simon, Phys. Rev. Lett. **51**, 2167 (1983).

[5] F. D. M. Haldane, Phys. Rev. Lett. **61**, 2015 (1988).

[6] E. Tang, J.-W. Mei, and X.-G. Wen, Phys. Rev. Lett. **106**, 236802 (2011).

[7] K. Sun, Z. Gu, H. Katsura, and S. Das Sarma, Phys.

Rev. Lett. **106**, 236803 (2011).

[8] T. Neupert, L. Santos, C. Chamon, and C. Mudry, Phys. Rev. Lett. **106**, 236804 (2011).

[9] D. N. Sheng, Z.-C. Gu, K. Sun, and L. Sheng, Nature Comm. **2**, 389 (2011).

[10] N. Regnault and B. A. Bernevig, Phys. Rev. X **1**, 021014 (2011).

[11] Y.-F. Wang, Z.-C. Gu, C.-D. Gong, and D. N. Sheng, Phys. Rev. Lett. **107**, 146803 (2011).

[12] X.-L. Qi, Phys. Rev. Lett. **107**, 126803 (2011).

[13] B. A. Bernevig and N. Regnault, Phys. Rev. B **85**, 075128 (2012).

[14] Y.-F. Wang, H. Yao, Z.-C. Gu, C.-D. Gong, and D. N. Sheng, Phys. Rev. Lett. **108**, 126805 (2012).

[15] Y.-L. Wu, B. A. Bernevig, and N. Regnault, Phys. Rev. B **85**, 075116 (2012).

[16] S. A. Parameswaran, R. Roy, and S. L. Sondhi, Phys. Rev. B **85**, 241308 (R) (2012).

[17] M. O. Goerbig, Eur. Phys. J. B **85**, 15 (2012).

[18] G. Murthy and R. Shankar, Phys. Rev. B **86**, 195146 (2012).

[19] C. H. Lee, R. Thomale, and X.-L. Qi, Phys. Rev. B **88**, 035101 (2013).

[20] J. W. F. Venderbos, S. Kourtis, J. van den Brink, and M. Daghofer, Phys. Rev. Lett. **108**, 126405 (2012).

[21] N. R. Cooper and J. Dalibard, Phys. Rev. Lett. **110**, 185301 (2013).

[22] Y.-L. Wu, N. Regnault, and B. A. Bernevig, Phys. Rev. B **86**, 085129 (2012).

[23] T. Liu, C. Repellin, B. A. Bernevig, and N. Regnault, Phys. Rev. B **87**, 205136 (2013).

[24] Y.-H. Wu, J. K. Jain, and K. Sun, Phys. Rev. B **86**, 165129 (2012).

[25] T. Scaffidi and G. Möller, Phys. Rev. Lett. **109**, 246805 (2012).

[26] Z. Liu and E. J. Bergholtz, Phys. Rev. B **87**, 035306 (2013).

[27] C. H. Lee and X.-L. Qi, arXiv:1308.6831 (2013).

[28] S. A. Parameswaran, R. Roy, and S. L. Sondhi, Comptes Rendus Physique, ISSN 1631-0705 (2013).

[29] E. J. Bergholtz and Z. Liu, Int. J. Mod. Phys. B **27**, 1330017 (2013).

[30] Y.-F. Wang, H. Yao, C.-D. Gong, and D. N. Sheng, Phys. Rev. B **86**, 201101 (2012).

[31] M. Trescher and E. J. Bergholtz, Phys. Rev. B **86**, 241111 (2012).

[32] S. Yang, Z.-C. Gu, K. Sun and S. Das Sarma, Phys. Rev. B **86**, 241112 (2012).

[33] Z. Liu, E. J. Bergholtz, H. Fan, and A. M. Läuchli, Phys. Rev. Lett. **109**, 186805 (2012).

[34] A. Sterdyniak, C. Repellin, B. A. Bernevig, and N. Regnault, Phys. Rev. B **87**, 205137 (2013).

[35] Y.-L. Wu, N. Regnault, and B. A. Bernevig, Phys. Rev. Lett. **110**, 106802 (2013).

[36] B. I. Halperin, Helv. Phys. Acta **56**, 75 (1983).

[37] M. Barkeshli and X.-L. Qi, Phys. Rev. X **2**, 031013 (2012).

[38] R. E. Peierls, Z. Phys. Rev. **80**, 763 (1933).

[39] P. G. Harper, Proc. Phys. Soc. London, Sect. A **68**, 874 (1955).

[40] G. H. Wannier, Rev. Mod. Phys. **34**, 645 (1962).

[41] M. Ya. Azbel, Zh. Eksp. Teor. Fiz. **46**, 939 (1964) [Sov. Phys. JETP **19**, 634 (1964)].

[42] D. R. Hofstadter, Phys. Rev. B **14**, 2239 (1976).

[43] See the Supplemental Material.

[44] R. B. Laughlin, Phys. Rev. Lett. **50** 1395 (1983).

[45] J. K. Jain, Phys. Rev. Lett. **63**, 199 (1989).

[46] F. D. M. Haldane, Phys. Rev. Lett. **55**, 2095 (1985).

[47] I. A. McDonald, Phys. Rev. B **51**, 10851 (1995).

[48] The small $V_{\sigma\tau}^B$ term has been added slightly to lift the degeneracies between some energy levels, which increases the efficiency of convergence in exact diagonalization.

[49] S. A. Kivelson, E. Fradkin, and V. J. Emery, Nature **393**, 550 (1998).

[50] E. Fradkin, S. A. Kivelson, M. J. Lawler, J. P. Eisenstein, and A. Mackenzie, Ann. Rev. Cond. Matt. Phys. **1**, 153 (2010).

[51] One can also choose the Hamiltonian such that the Halperin 330 state is realized. It is unclear whether this is related to the pseudopotential Hamiltonian proposed in Ref. [27].

[52] M. Barkeshli, C.-M. Jian, and X.-L. Qi, Phy. Rev. B **87**, 045130 (2013).

[53] M. Barkeshli and X.-L. Qi arXiv:1302.2673 (2013).

[54] M. Cheng, Phys. Rev. B **86**, 195126 (2012).

[55] N. H. Lindner, E. Berg, G. Refael, and A. Stern, Phys. Rev. X **2**, 041002 (2012).

[56] D. J. Clarke, J. Alicea, and K. Shtengel, Nature Comm. **4**, 1348 (2013).

[57] A. Vaezi, Phys. Rev. B **87**, 035132 (2013).

[58] J. Dalibard, F. Gerbier, G. Juzeliūnas, and P. Öhberg, Rev. Mod. Phys. **83**, 1523 (2011)

[59] N. Goldman, G. Juzeliūnas, P. Öhberg, and I. Spielman, arXiv:1308.6533 (2013).

[60] M. Aidelsburger, M. Atala, M. Lohse, J. T. Barreiro, B. Paredes, and I. Bloch, Phys. Rev. Lett. **111**, 185301 (2013).

[61] H. Miyake, G. A. Siviloglou, C. J. Kennedy, W. C. Burton, and W. Ketterle, Phys. Rev. Lett. **111**, 185302 (2013).

[62] J. Koch, A. A. Houck, K. L. Hur, and S. M. Girvin, Phys. Rev. A **82**, 043811 (2010).

[63] R. O. Umucalilar and I. Carusotto, Phys. Rev. A **84**, 043804 (2011).

[64] M. Hafezi, E. A. Demler, M. D. Lukin, and J. M. Taylor, Nature Phys. **7**, 907 (2011).

[65] A. A. Houck, H. E. Tureci, and J. Koch, Nature Phys. **8**, 292 (2012).

[66] R. O. Umucalilar and I. Carusotto, Phys. Rev. Lett. **108**, 206809 (2012).

[67] E. Kapit and S. H. Simon, Phys. Rev. **B** 88, 184409 (2013).

[68] M. Hafezi, P. Adhikari, and J. M. Taylor, arXiv:1308.0225 (2013).

[69] E. Kapit, M. Hafezi, and S. H. Simon, arXiv:1402.6847 (2014).

[70] M. Hafezi, S. Mittal, J. Fan, A. Migdall, and J. M. Taylor, Nature Photon. **7**, 1001 (2013).

[71] M. C. Rechtsman, J. M. Zeuner, Y. Plotnik, Y. Lumer, D. Podolsky, F. Dreisow, S. Nolte, M. Segev, and A. Szameit, Nature **496**, 196 (2013).

[72] N. Jia, A. Sommer, D. Schuster, and J. Simon, arXiv:1309.0878 (2013).

[73] S. Mittal, J. Fan, S. Faez, A. Migdall, J. M. Taylor, and M. Hafezi, arXiv:1404.0090 (2014).